



## Experimental investigation of Fe-clay/organic interactions under asteroidal conditions

J.-C. Viennet, Corentin Le Guillou, L. Remusat, F. Baron, L. Delbes, Anne-Marie Blanchenet, B. Laurent, I. Criouet, S. Bernard

### ► To cite this version:

J.-C. Viennet, Corentin Le Guillou, L. Remusat, F. Baron, L. Delbes, et al.. Experimental investigation of Fe-clay/organic interactions under asteroidal conditions. *Geochimica et Cosmochimica Acta*, 2021, *Geochimica et Cosmochimica Acta*, 318, pp.352-365. 10.1016/j.gca.2021.12.002 . hal-03487101

**HAL Id: hal-03487101**

**<https://hal.univ-lille.fr/hal-03487101>**

Submitted on 21 Jun 2022

**HAL** is a multi-disciplinary open access archive for the deposit and dissemination of scientific research documents, whether they are published or not. The documents may come from teaching and research institutions in France or abroad, or from public or private research centers.

L'archive ouverte pluridisciplinaire **HAL**, est destinée au dépôt et à la diffusion de documents scientifiques de niveau recherche, publiés ou non, émanant des établissements d'enseignement et de recherche français ou étrangers, des laboratoires publics ou privés.

# **Experimental investigation of Fe-clay/organic interactions under asteroidal conditions**

J.-C. Viennet<sup>1</sup>, C. Le Guillou<sup>2</sup>, L. Remusat<sup>1</sup>, F. Baron<sup>3</sup>, L. Delbes<sup>1</sup>, A.M. Blanchenet<sup>2</sup>, B.

Laurent<sup>1</sup>, I. Criouet<sup>1</sup>, S. Bernard<sup>1</sup>

<sup>1</sup> Muséum National d'Histoire Naturelle, Sorbonne Université, UMR CNRS 7590, Institut de minéralogie, de physique des matériaux et de cosmochimie, Paris, France.

<sup>2</sup> Univ. Lille, CNRS, INRA, ENSCL, UMR 8207 - UMET - Unité Matériaux et Transformations, F-59000 Lille, France.

<sup>3</sup> Institut de Chimie des Milieux et Matériaux de Poitiers (IC2MP), UMR 7285 CNRS, Université de Poitiers, F-86073 Poitiers Cedex 9, France.

\* Corresponding author at: Muséum National d'Histoire Naturelle, Sorbonne Université, CNRS, UMR 7590, Institut de Minéralogie, Physique des Matériaux et Cosmochimie, Paris, France.

E-mail address: jean.christophe.viennet25@gmail.com (J.-C. Viennet).

## **Keywords**

Clay minerals, Organic-mineral interaction; Hydrothermal alteration, Asteroids, Carbonaceous chondrites.

## Abstract

Carbonaceous chondrites contain both soluble and insoluble organic materials (SOM and IOM) which may have been produced in different environments via different processes or share possible genetic relationships. The SOM may have been produced from IOM during hydrothermal episodes on asteroids, and *vice versa*. The potential role played by the mineral matrix during these episodes (clay minerals of variable crystallinity) remains to be constrained. Here, we exposed a mixture of formaldehyde and glycolaldehyde with ammonia-bearing liquid water together with Fe-rich smectitic minerals to hydrothermal conditions mimicking asteroidal conditions. We used both amorphous gel of smectite or crystalline smectites in order to understand the influence of the crystallinity on the evolution of OM. The organo-mineral experimental residues were characterized at a multiple length scales using X-ray diffraction and microscopy/spectroscopic tools. Results evidence that some IOM polymerizes/condenses in the absence of Fe-rich smectites. Yet, the presence of Fe-rich smectites inhibits this production of IOM. Indeed, the interactions between the SOM and clay surfaces (interlayers or edges) reduce the concentration of SOM available for polymerization/condensation reactions, a necessary step for the production of IOM. In addition, the presence of OM disorganizes the crystallization of the Fe-rich amorphous silicates, leading to smaller crystal sized particles exhibiting a lower permanent charge. This might suggest that the smectite permanent charge distribution may help better constraining the origin and evolution of chondritic clay minerals. Altogether, the present study sheds new light on the organo-mineral interactions having occurred during hydrothermal episodes onto/within chondritic asteroids. Indeed, IOM formation from OM-rich aqueous fluids does not occur during the alteration of amorphous silicates. This would mean that IOM is either produced within pockets free of clay minerals or initially accreted as IOM-rich grain. Last, about ~50 wt.% of the initial C could not be removed from the clay minerals at the end of the experiments using classical solvent extraction protocols, demonstrating that a high fraction of the SOM in carbonaceous chondrites may have been overlooked.

## 1. Introduction

Carbonaceous chondrites (CC) contain up to 5 wt. % of organic matter (OM) dominated by an insoluble fraction (IOM - 75 to 90 wt. %) associated with a minor soluble fraction (SOM - 10 to 25 wt%) (Robert and Epstein, 1982; Pearson et al., 2006; Alexander et al., 2007, 2017; Sephton, 2014; Remusat, 2015). While the SOM is composed of a diversity of small organic molecules (such as carboxylic acids, amino acids, nucleobases, polycyclic aromatic hydrocarbons, sugars...) (Pizzarello et al., 2006), the IOM consists in high molecular weight molecules made of aromatic units and short aliphatic chains rich in hetero-elements (Cody and Alexander, 2005; Remusat et al., 2005a; Remusat et al., 2019; Alexander et al., 2007; Derenne and Robert, 2010; Vinogradoff et al., 2017).

The possible genetic relationships between the SOM and the IOM remains a subject of investigations, notably because these compounds, potentially produced in different environments via different processes (Kerridge, 1993; Remusat et al., 2009; Aléon, 2010), have undergone multiple processes since their accretion onto/by parent bodies (McSween, 1979; Brearley, 2006; Danger et al., 2021). In fact, the presence of mineral products of hydrothermal alteration (e.g., smectite and/or serpentine phyllosilicates, carbonates and/or sulfides) have been reported in all CCs (Brearley, 2006; Le Guillou and Brearley, 2014; Le Guillou et al., 2014; King et al., 2015; Yesiltas and Kebukawa, 2016; Vinogradoff et al., 2017; Changela et al., 2018; Dionnet et al., 2018; Nittler et al., 2019; Vollmer et al., 2020).

Recent laboratory experiments demonstrated that IOM may form from SOM under asteroidal hydrothermal conditions. In fact, when exposed to 150°C, a mixture of formaldehyde and glycolaldehyde within liquid water containing ammonia will evolve into a diversity of soluble

69 compounds together with macromolecular organic solids sharing similarities with the chondritic  
70 IOM through formose and condensation reactions (Cody et al., 2011; Kebukawa et al., 2013, 2017,  
71 2020; Kebukawa and Cody, 2015). Similar results were obtained using HMT  
72 (Hexamethylenetetramine - Vinogradoff et al., (2018)), i.e. the main product component of  
73 interstellar ice analogs (Bernstein et al., 1995; Cottin et al., 2001; Vinogradoff et al., 2011). This  
74 molecule decomposes into formaldehyde and ammonia in water at temperature  $> 70^{\circ}\text{C}$  (Meissner  
75 et al., 1954; Blazzevjic et al., 1979) producing solid macromolecular carbon insoluble in organic  
76 solvents within a few days at  $150^{\circ}\text{C}$  (Vinogradoff et al., 2018).

77 Yet, the possible role played by smectites in the production of IOM from SOM under asteroidal  
78 hydrothermal conditions (i.e.  $\sim 50$  to  $\sim 200^{\circ}\text{C}$  - Brearley, (2006)) requires further investigations. In  
79 fact, smectites closely associated to OM have been reported in chondrite matrices (Pearson et al.,  
80 2006; Garvie and Buseck, 2007; Le Guillou and Brearley, 2014; Le Guillou et al., 2015; Yesiltas  
81 and Kebukawa, 2016; Vinogradoff et al., 2017; Changela et al., 2018) and recent experimental  
82 studies have revealed that smectitic clay minerals may have a strong influence on organic reactions  
83 under hydrothermal conditions (Viennet et al., 2019, 2020; Vinogradoff et al., 2020a, b). While  
84 OM may influence smectite crystallization (Jacquemot et al., 2019), clay minerals may  
85 promote/catalyze various organic reactions (including cyclization, dehydration, Michael-  
86 addition...) even at temperatures below  $100^{\circ}\text{C}$  (Nagendrappa, 2011; Nagendrappa and Chowreddy,  
87 2021). This is particularly the case of Fe-rich clay minerals, because the reactivity of some organic  
88 reactions in liquid water are enhanced in appropriate redox conditions (Lewan, 1997; Seewald,  
89 2001; McCollom and Seewald, 2006; Pan et al., 2009; McCollom et al., 2010; Lewan and Roy,  
90 2011; Foustoukos and Stern, 2012; McCollom, 2013).

91 Here, we document the hydrothermal evolution of a mixture of formaldehyde and glycolaldehyde

within liquid water containing ammonia in the presence of Fe-rich smectitic phase, either amorphous or crystalline. The organo-mineral experimental residues were characterized at a multiple length scale using X-ray diffraction and advanced microscopy and spectroscopy tools, including infrared spectroscopic, scanning electron microscopy, scanning transmission X-ray microscopy coupled with X-ray absorption near edge spectroscopy and scanning transmission electron microscopy coupled with energy dispersive X-ray spectroscopy.

## **2. Materials and methods**

### **2.1. Starting Materials**

The organic starting material used for the present experiments is similar to that of previous studies (Cody et al., 2011; Kebukawa et al., 2013, 2017, 2020; Kebukawa and Cody, 2015). As done by Ricardo (2004), paraformaldehyde (1.5 mmol - 45 mg - Sigma Aldrich) and glycolaldehyde (1.5 mmol - 45 mg - Sigma Aldrich) were mixed within 2mL of pure water in which was added 12 mg of Ca(OH)<sub>2</sub> (Sigma Aldrich). Nitrogen was added as NH<sub>4</sub>OH (20 µl - 14.8N - Sigma Aldrich) establishing the initial atomic N/C value at 0.1 (33 wt.% of C and 3.8 wt.% of N).

Pure nontronite (Na<sub>0.4</sub>(Fe(III)<sub>2</sub>)(Si<sub>3.6</sub>Fe(III)<sub>0.4</sub>)O<sub>10</sub>(OH)<sub>2</sub>) was used as the Fe-rich smectitic mineral phase. An amorphous gel of nontronite was obtained by mixing SiNa<sub>2</sub>O<sub>3</sub>.5H<sub>2</sub>O (Sigma Aldrich) and Fe(III)Cl<sub>3</sub>.6H<sub>2</sub>O (Sigma Aldrich) following the procedure detailed in Baron et al. (2016) and Petit et al. (2017). Salts and cations in excess were removed via filtration. The crystalline nontronite was synthesized by submitting the amorphous gel of nontronite to hydrothermal conditions (3 days at 150°C - Water/Gel of 3/50) in PTFE Parr© reactors. Washing with dichloromethane was performed to remove potential organic contamination. These mineral starting materials were then dried at room temperature (~ 25°C) over a day.

## 2.2. Laboratory Experiments

A first experiment was conducted in the absence of mineral. Confirming previous studies (Kebukawa and Cody, 2015), this experiment led to the production of IOM. For the experiments with minerals, 100 mg of either the crystalline nontronite or the nontronite gel were added to the 2 mL solution containing the organic mixture. These organo-mineral mixtures were introduced within titanium Parr© reactors loaded with 1 bar of Ar before closure and placed at 150 °C for 3 days (making them reach an authigenic water pressure of 5 bars). Note that, the NH<sub>4</sub>OH solution was introduced the latest, just before closing the reactors to avoid degassing of NH<sub>3</sub>(g). In agreement with previous studies (Baron et al., 2016), after 3 days at 150 °C, the amorphous gel crystallizes in the absence of the organic mixture (Baron et al., 2016) and the IOM yield is maximal in the absence of mineral (Kebukawa and Cody, 2015).

The experimental residues were filtered and washed with ultrapure water and dichloromethane (DCM) to remove the free soluble organic compounds (i.e. the soluble organic compounds not retained by the solid phases) and dried under vacuum ( $3 \cdot 10^{-4}$  mBar) before characterization. Ten milligrams of each solid residue were subjected to HF/HCl dissolution protocols (Remusat et al., 2005b) to isolate the IOM possibly produced during the experiments. A 2:1 volume ratio HF/HCl (16/2 N) treatment was conducted for 24 hours, at room temperature. Note that, no IOM was recovered from the experiments with minerals. Control experiments without the organic mixture were also conducted to ensure the absence of contamination (Table S1 - Figure S1).

## 2.3. Characterization techniques

### 2.3.1. *Elemental analyses*

Total carbon and nitrogen contents were determined using a Flash2000, Thermo Fisher, elemental analyzer operating at the Service de Spectrometry de Masse Isotopique du Museum (SSMIM) at MNHN in Paris (France). A mass of 1 mg of each residue was combusted under oxygen/helium flux at 1020°C. The N<sub>2</sub> and CO<sub>2</sub> released by combustion were separated by a chromatography column and quantified using a thermal conductivity detector. Alanine was used as standard giving uncertainties at 0.1 wt. % for N and 0.2 wt. % for C.

### 2.3.2. *XRD*

The X-ray diffraction (XRD) patterns were obtained on a Panalytical X'pert Pro MPD 2 circles operating at IMPMC (Paris, France) The divergence slit, the anti-scatter slit and the two Soller slits were set at 0.5°, 1°, 0.04° and 0.04 radian, respectively. The bulk XRD measurements were performed on powder preparations throughout the 3-65 °2θ CoKα<sub>1,2</sub> angular range (step size of 0.033 °2θ, counting time per step of 250 ms). The experiments dedicated to OM location were performed on oriented preparations at both atmospheric pressure and under vacuum (3.10<sup>-4</sup> atmosphere) at 20 °C using an Anton Parr HTK 1200 oven coupled to an EDWARDS RV3 pump throughout the 3-12 °2θ CoKα<sub>1,2</sub> angular range (step size of 0.033 °2θ, counting time per step of 250 ms).

### 2.3.3. *MIR*

Mid-infrared (MIR) spectra were recorded in the 400-4000 cm<sup>-1</sup> range with a 4 cm<sup>-1</sup> resolution using a Nicolet 6700 FTIR spectrometer (IMPMC, Paris) equipped with a KBr beamsplitter and a DTGS-KBr detector, under ambient conditions by averaging 200 scans obtained in attenuated total reflectance (ATR) geometry using a Specac Quest ATR device fitted with a diamond internal reflection element. Transmission MIR spectra were obtained in the 400-4000 cm<sup>-1</sup> range with a 4



cm<sup>-1</sup> resolution using a Nicolet™ iS™ 50 FTIR spectrometer (IMPMC, Paris) equipped with a KBr beamsplitter, an Ever-Glo source and a DTGS-KBr detector, by averaging 200 scans from KBr pellets dried at 110°C obtained by mixing 1 mg of samples with 150 mg of KBr (Sigma Aldrich).

#### 2.3.4. SEM

Scanning electron microscopy (SEM) investigations were performed on powders deposited on carbon tape using the SEM-FEG ZEISS ULTRA 55 (IMPMC, Paris) equipped with a Bruker EDS QUANTAX detector (Bruker Corporation, Houston, TX, USA). Images shown here (secondary electrons) were collected using an acceleration voltage below 2 kV, thereby preventing irradiation damages.

#### 2.3.5. Cryo-ultramicrotomy

Cryo-ultramicrotome sections (100 nm thick) were prepared for X-ray absorption near edge structure (XANES) and transmission electron microscopy (STEM) investigations using a Leica cryo-ultramicrotome at UMET (Lille, France) following a recently developed protocol (Jacquemot et al., 2019; Viennet et al., 2019, 2020). Powders of experimental residues were mixed with 0.1 ml of deionized water, then a drop of the mixture was frozen in liquid nitrogen at -120 °C and cut. The ultrathin slices of residues were then deposited on holey carbon film TEM grids (coated with a ~3 nm chromium layer).

#### 2.3.6. XANES

XANES data were collected using the HERMES STXM beamline at the synchrotron SOLEIL (Belkhou et al., 2015; Swaraj et al., 2017). Beamline optical elements were exposed to a continuous flow of pure O<sub>2</sub> to remove carbon contamination. Energy calibration was done before measurements using the well-resolved 3p Rydberg peak of gaseous CO<sub>2</sub> at 294.96 eV. XANES data were extracted from image stacks collected at energy increments of 0.1 eV over the carbon

(270–350 eV) absorption range with a dwell time of  $\leq 1$  ms per pixel to prevent irradiation damage (Wang et al., 2009). Alignment of stack images and extraction of XANES spectra were done using the aXis2000 software. The C-XANES spectra shown here correspond to homogenous carbon-rich areas of several hundreds of square nanometers. Following the method described in Le Guillou et al. (2018), background was subtracted using a power law before spectra were normalized to the carbon quantity by integrating the spectra from the pre-edge region up to the mean ionization energy (e.g. 282.0-291.5 eV at the C K edge).

### 2.3.7. TEM

Scanning transmission electron microscopy (STEM) and electron dispersive spectroscopy (EDS) mapping were performed using a Thermofisher Titan Themis 300 microscope operated at 300 keV, at the “centre commun de microscopie – CCM” at the University of Lille. High resolution images were obtained in STEM mode using the high angle annular dark field detector (HAADF), a convergence angle of 20 mrad, a camera length of  $\sim 150$  mm, a beam current below 200 pA and a dwell time between 5 and 10  $\mu$ s. Hyperspectral EDS data were obtained using the super-X detector system equipped with four windowless silicon drift detectors. The probe current was set at 600 pA with a dwell time of 2  $\mu$ s per pixel. A key aspect is the post-acquisition processing of the hyperspectral data, performed using the Hyperspy python-based package (de la Pena et al., 2017). The EDS spectrum at each pixel was fitted by a combination of Gaussian functions for the X-ray lines and a 6<sup>th</sup> order polynomial function for the background. Quantification was achieved using the integrated intensities of the Gaussian through the Cliff-Lorimer method (Cliff and Lorimer, 1975), using experimentally determined k-factors. The thickness x density product strongly affects the X-ray reabsorption of the light elements (O, Fe\_L). It was determined using the two-lines

204 method (Morris, 1980), which compares the quantification obtained from the Iron L-lines and Iron  
205 K-lines and accurate absorption correction was performed.

206

### 3. Results

#### 3.1. MIR spectra of the SOM

In the following, we focus on the characterization of the DCM-washed solid residues. Of note, only the residue produced in the absence of minerals contained IOM, although the free soluble organic compounds extracted using DCM exhibit very similar MIR spectra (Figure 1). The spectra exhibit stretching of O-H or N-H bonds at 3370 and 3200  $\text{cm}^{-1}$ , of aliphatic C-H at 2959  $\text{cm}^{-1}$  and 2920  $\text{cm}^{-1}$ , of C-H of -O-CH<sub>x</sub> bonds at 2851  $\text{cm}^{-1}$  (Kebukawa et al., 2020), N-H bonds in amide at 1567-1580  $\text{cm}^{-1}$ , of C-H, C-N, O-H bonds at 1412, 1382, 1315  $\text{cm}^{-1}$ , of C-O in alkoxy at 1043, 1076, 1120  $\text{cm}^{-1}$ , and C-H bending in alkene at 928 and 770  $\text{cm}^{-1}$ . Note that the MIR spectra of the initial OM exhibit important differences than for the free soluble organic compounds demonstrating the OM evolution due to the experimental hydrothermalism.

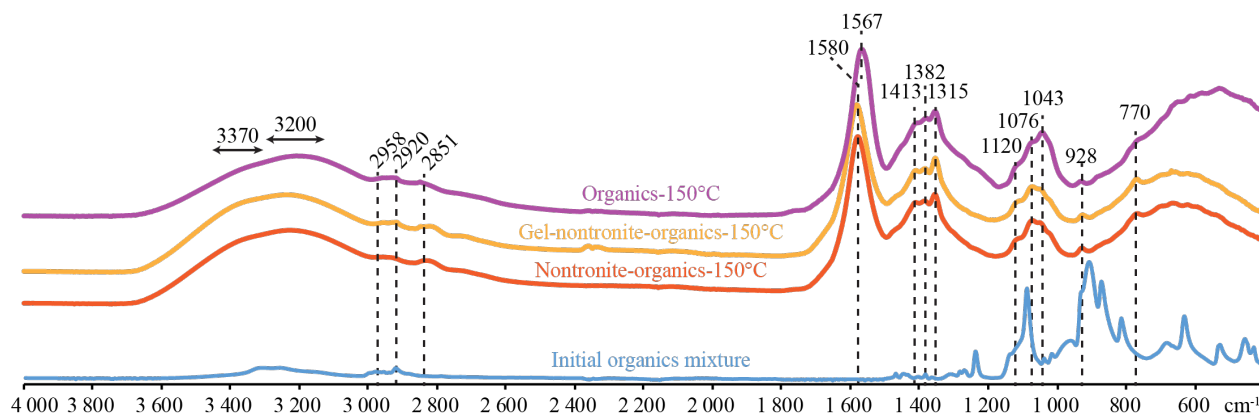


**Figure 1:** ATR-MIR spectra of initial OM and of the free soluble organic compounds extracted using DCM from the experimental residues.

### 223 3.2. TOC and N/C

224 Here, we focus on the characterization of the DCM-washed solid residues of experiments. The  
 225 experiments conducted in the absence of minerals lead to the production of a solid organic residue  
 226 insoluble in organic solvents, i.e. to the production of IOM. This IOM contains 65 wt.% of carbon  
 227 (24 % of the initial mass of carbon) and 7.3 wt.% of nitrogen (22.8 % of the initial mass of nitrogen).  
 228 In contrast, no IOM was recovered after the dissolution of the silicates using acid demineralization.  
 229 The solid residues produced in the presence of the crystalline nontronite or in the presence of the  
 230 gel of nontronite contain 14.3 and 14.1 wt.% of carbon (54.3 and 50.1 % of the initial carbon,  
 231 respectively) and 2 and 1.9 wt% of nitrogen (64.4 and 56.2 % of the initial nitrogen, respectively).  
 232 This OM exhibits slightly higher N/C values (0.12) than those of the starting organic material and  
 233 of the IOM produced in the absence of minerals (0.10).

Starting Materials	Organic-150°C	Nontronite Organics	Gel-nontronite Organics
Initial mass of organic mixture (mg)	102	102	102
Initial mass of minerals (mg)	0	100	100
Final mass of solids (mg)	12.4	127.7	119.8
Initial % <sub>wt</sub> C	33.0	16.7	16.7
Final % <sub>wt</sub> C	64.8	14.5	13.2
Initial mass of C (mg)	33.7	33.7	33.7
Final mass of C (mg)	8.0	18.5	15.8
Percentage of initial C trapped (%)	23.8	54.9	47.0
Initial % <sub>wt</sub> N	3.8	1.9	1.9

Final % wt N	7.3	2.0	1.9
Initial mass of N (mg)	3.9	3.9	3.9
Final mass of N (mg)	0.9	2.5	2.2
Percentage of initial N trapped (%)	23.0	64.4	56.2
Final N/C of the solid residue	0.10	0.12	0.12
IOM	Yes	No	No

*Table 1: Carbon and nitrogen contents in solid experimental residues and N/C values.*

### 3.3. XRD

XRD provide information on the nature and crystallinity of the solid fraction of the residues (Figure 2). Nontronite is a smectite made of 2:1 layers composed of an octahedral sheet sandwiched between two tetrahedral sheets. Isomorphic substitution by a lower charge cation in the tetrahedral sheets ( $\text{Si}^{4+}$  substitution by  $\text{Fe}^{3+}$ ) induces a negative charge, called “permanent charge”. The latter is compensated by exchangeable cations present either within the interlayer space (originally  $\text{Na}^+$  here) or on the basal planes. In addition, other charges due to crystal defects, such as silanol bonds are present on the edges of the clay minerals sheets.

In the absence of the organic mixture, the gel of nontronite (initially amorphous, as indicated by its XRD pattern – Figure 2) crystallizes into a low charge nontronite, as attested by the XRD peaks at 4.55, 3.15, 2.59, 1.73 and 1.525 Å corresponding to the 0.2.11, 004, 13.20, 15.24.31 and 06.33 reflections of the crystalline nontronite (Baron et al., 2016). In contrast, in the presence of the organic mixture, the nontronite gel does not crystallize that well. The XRD pattern of the solid residue do not show the 001 reflection. The wide peaks at 4.37, 2.57 and 1.537 Å correspond to the 0.2.11, 13.20 and 06.33 reflections of a poorly crystalline nontronite (Baron et al., 2019). The

crystallinity of the crystalline nontronite also decreases during the experiments conducted in the presence of the organic mixture as evidenced by the broadening of the hkl reflections. In addition, the 001 reflection of the solid residue is shifted to 18.00 Å, likely due to mixed-layer stacking and/or trapping of OM into its interlayer space (Laird, 1994; Lagaly et al., 2013; Viennet et al., 2015, 2016, 2019, 2020; Gautier et al., 2017). Such trapping of organic carbon within the interlayer spaces of the nontronites seems to be confirmed by XRD measurements performed under vacuum (Figure 3). In fact, under vacuum, the distance corresponding to the 001 reflection of the residues produced in the presence of the organic mixture do not collapse, in contrast to that of the crystalline nontronite that were never exposed to the organic mixture. Indeed, only small shifts of their 001 reflections attest that the interlayer spaces of these smectites are locked by organic compounds (Viennet et al., 2019, 2020).

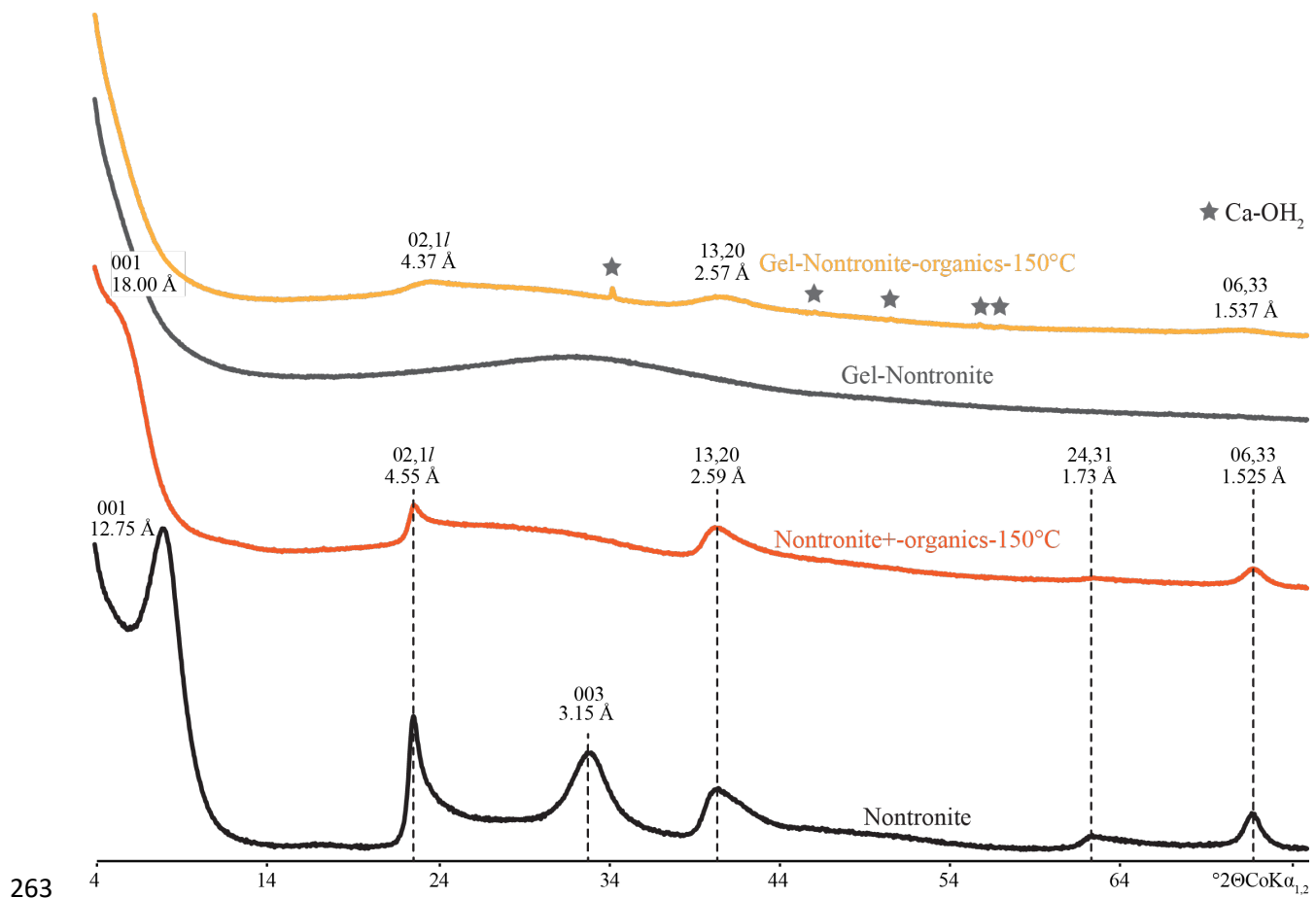


**Figure 2:** XRD patterns of the starting gel of nontronite, the starting nontronite and the solid residues of experiments. The small peaks at 3.03, 2.49, 2.28, 2.09, 1.91, 1.87 Å (grey stars) are attributed to  $\text{CaOH}_2$ .



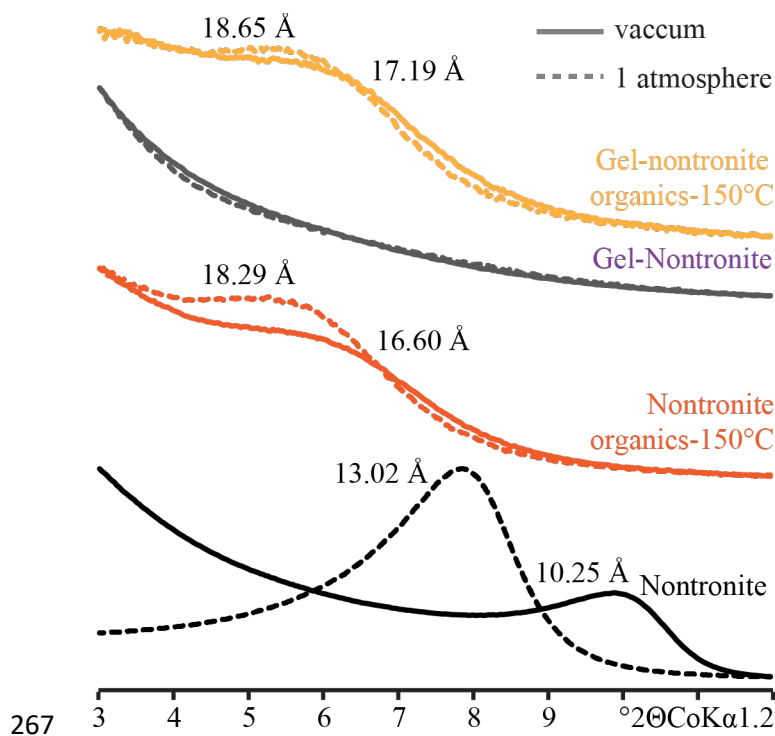


**Figure 3:** XRD patterns under ambient pressure and under vacuum of the starting gel of nontronite, the starting nontronite, and the solid residues of experiments. Note that the 001 reflection of the residues produced in the presence of the organic mixture do not shift to  $\sim 10 \text{ \AA}$  under vacuum, indicating the presence of OM within the interlayer space of the nontronites.

### 3.4. MIR

Transmission-MIR investigations in the  $400\text{-}1300 \text{ cm}^{-1}$  range confirm that, the crystalline nontronite is a low charge smectite (Figure 4). In fact, spectra show sharp bands attributed to stretching of Si-O ( $1008 \text{ cm}^{-1}$ ), bending of  $\text{Fe}^{3+}_2\text{-OH}$  ( $816 \text{ cm}^{-1}$ ), symmetrical stretching of Si-O-Si ( $780 \text{ cm}^{-1}$ ),  $^{[4]}\text{Fe(III)-O}$  vibrations ( $707 \text{ cm}^{-1}$ ),  $^{[6]}\text{Fe(III)-O}_{\text{apical}}$  vibrations ( $677 \text{ cm}^{-1}$ ) and Si-O<sub>apical</sub>- $^{[6]}\text{Fe(III)}$  vibrations (around  $600 \text{ cm}^{-1}$ ) (Farmer, 1974; Baron et al., 2016). Of note, below  $600 \text{ cm}^{-1}$  and at  $840 \text{ cm}^{-1}$ , the attribution of the vibration bands remains complex (Baron et al., 2016). The

band at  $3630\text{ cm}^{-1}$  corresponds to the OH stretching vibrations of water molecules weakly bonded to the oxygen of the silicate lattice (Figure 4, Farmer and Russell, 1971). In addition, the bands at  $1632$ ,  $3232$  and  $3353\text{ cm}^{-1}$ , correspond to the vibrations of OH bonds in  $\text{H}_2\text{O}$ . The MIR spectra of the solid residues produced in the presence of the organic mixture exhibit the main absorption bands of nontronite, but these bands are rather wide compared to the sharp bands of crystalline nontronite, also indicating a lower degree of crystallinity (Baron et al., 2016). Plus, the bands attributed to the stretching of Si-O bonds are shifted at  $1028$  and  $1015\text{ cm}^{-1}$  for the residues produced with the crystalline nontronite and with the gel of nontronite, respectively, which can be explained by a slightly lower charge compared to that of the starting nontronite (Baron et al., 2016). A lower charge may also explain the lower intensity of the band at  $677\text{ cm}^{-1}$  and the higher intensity of the band at  $707\text{ cm}^{-1}$ , attributed to  $^{[4]}\text{Fe(III)-O}$  vibrations and  $^{[6]}\text{Fe(III)-O}_{\text{apical}}$  vibrations, respectively (Baron et al., 2016), while interactions with OM may explain the lower intensity of the band at  $815\text{ cm}^{-1}$ , attributed to the bending of  $\text{Fe}^{3+}_2\text{-OH}$  bonds. Compared to those of crystalline nontronite, the spectra of the residues produced in the presence of the organic mixture exhibit a broader and less intense band at  $3562\text{ cm}^{-1}$ , corresponding to the stretching of  $\text{Fe}^{3+}_2\text{-OH}$  in octahedral position (Baron et al., 2016). This evolution indicates either a lower degree of crystallinity and/or interactions of OM with the structural OH, which is consistent with transmission-MIR data. In addition, the band at  $3630\text{ cm}^{-1}$ , corresponding to the stretching of OH vibrations of water molecules weakly bonded to the oxygen of the silicate lattice (Farmer and Russell, 1971), is weaker in presence of organics, indicating either a lower degree of crystallinity and/or interactions of OM with the edges of smectites.

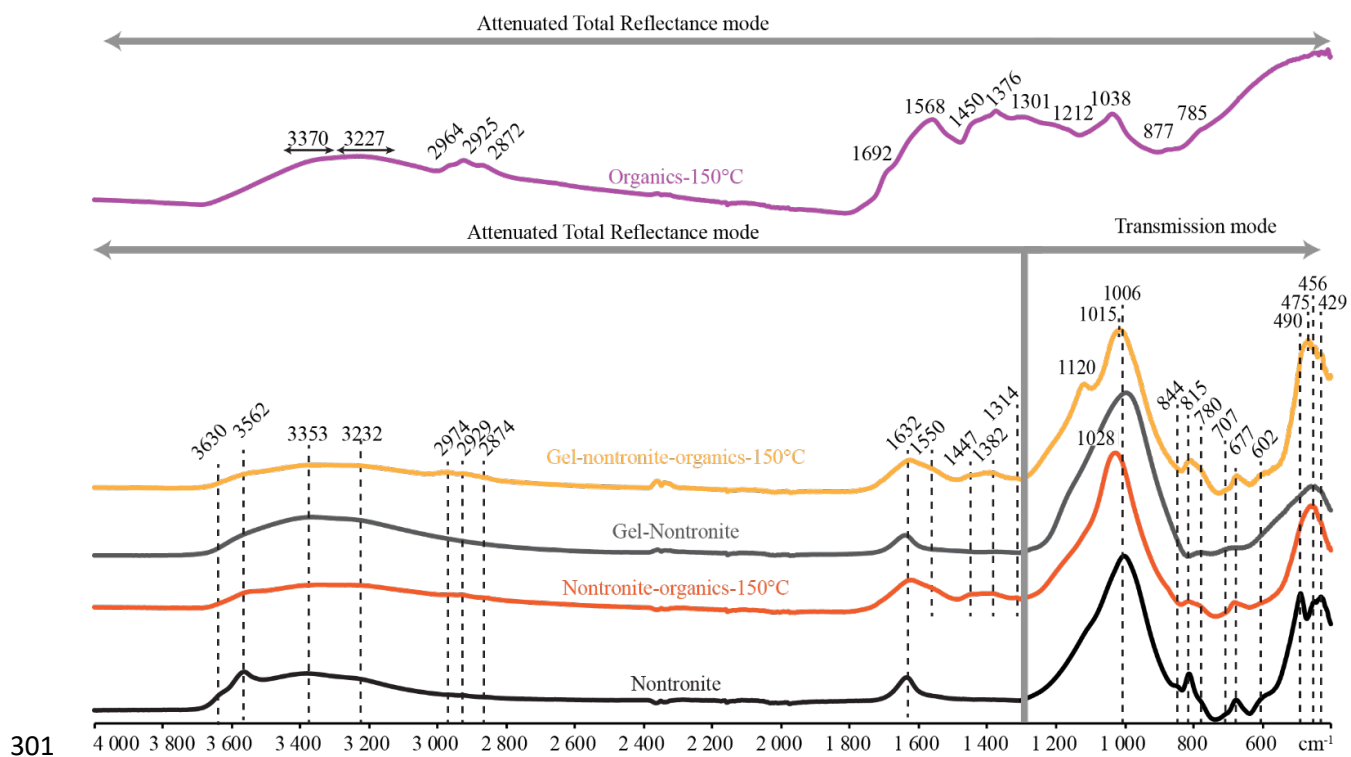


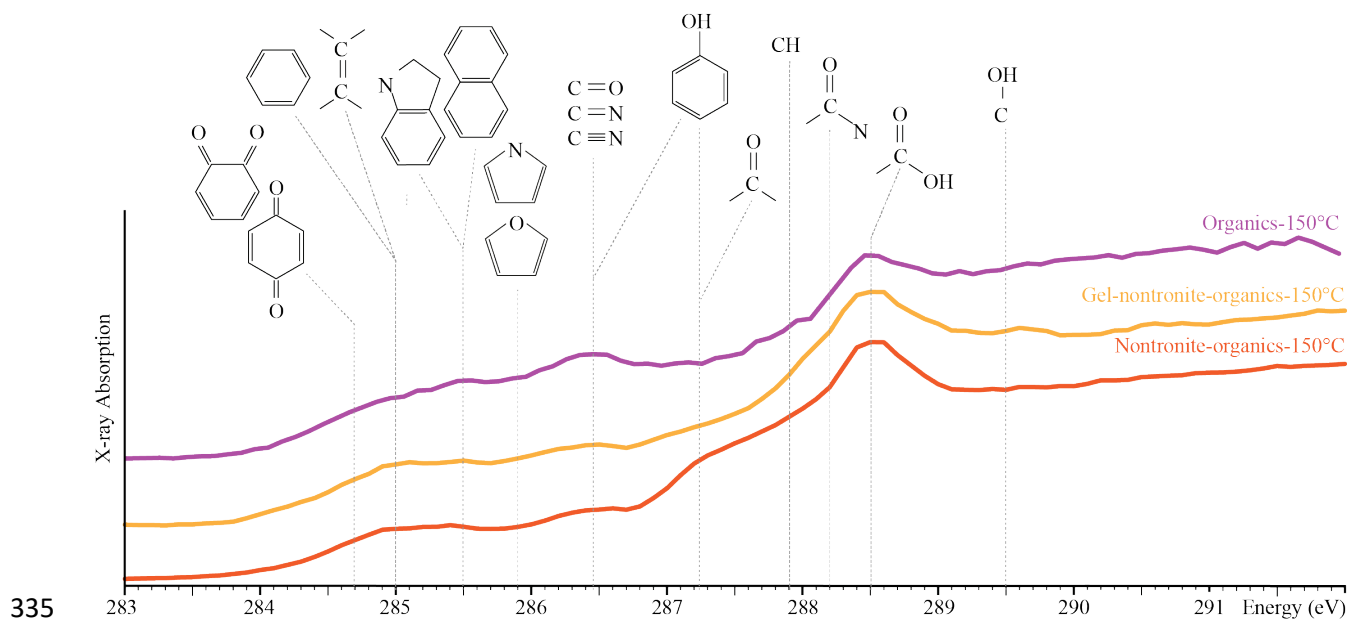
**Figure 4:** Infrared spectra in ATR mode from 4000 to 1300  $\text{cm}^{-1}$  and in transmission mode from 1300 to 400  $\text{cm}^{-1}$  of the pristine materials, of the organo-minerals residues and the mineral-free experiment (organics-150°C, in purple).

ATR-MIR spectra also provide information on the chemical nature of the organic fraction of the residues (Figure 4). In addition to a large band centered at 3227  $\text{cm}^{-1}$  attributed to O-H bonds, the spectrum of the IOM produced in the absence of minerals shows bands at 1376 and 1450  $\text{cm}^{-1}$  and at 2872, 2925 and 2964  $\text{cm}^{-1}$  attributed to the bending and stretching of aliphatic C-H, bands at 785 and 877  $\text{cm}^{-1}$  attributed to the bending of aromatic C-H, bands at 1038, 1212 and 1301  $\text{cm}^{-1}$  attributed to the stretching of alcohol C-O, a band at 1692  $\text{cm}^{-1}$  attributed to the stretching of amide/ester C=O and a band at 1556  $\text{cm}^{-1}$  attributed to the bending of amide N-H (Bernard et al., 2015). In contrast, the spectra of the organic compounds trapped within the residues produced from

the organic mixture in the presence of the crystalline nontronite or the gel of nontronite show bands at 1383 and 1447  $\text{cm}^{-1}$  and at 2874, 2929 and 2974  $\text{cm}^{-1}$  attributed to the bending and stretching of aliphatic C-H (although the band at 1447  $\text{cm}^{-1}$  may also be attributed to  $\text{R-NH}_3^+$ ), a band at 1314  $\text{cm}^{-1}$  attributed to the bending vibration of phenol C-O, and a band at 1550  $\text{cm}^{-1}$  attributed to the bending of amide N-H (Yariv and Cross, 2001; Gautier et al., 2017; Viennet et al., 2019, 2020).

### 3.5. XANES

The XANES spectra collected at the carbon edge on ultramicrotome sections also provide information on the chemical nature of the organic fraction of the residues (Figure 5). The XANES spectrum of the IOM produced in the absence of minerals shows peaks attributed to aromatic and olefinic carbons (285.0 eV), conjugated aromatic cycles (285.5 eV), heterocycles (286.0 eV), amine/imine/cyano groups and/or ketone and phenol groups (286.5 eV), aliphatic carbons (287.9 eV), amide groups (288.2 eV) and carboxylic groups (288.5 eV) (Alleon et al., 2017; Le Guillou et al., 2018). No IOM was produced in the presence of the crystalline nontronite, the organic carbon trapped within the solid residue exhibits different spectrum, with peaks at the same energies indicating a roughly similar chemistry, although this carbon appears to contain a bit more aromatic and/or olefinic carbons (285.1 eV), more phenol carbons (287.2 eV) and a bit more aliphatic carbons (287.9-288.5 eV). The organic carbon trapped within the solid residue produced in the presence of the gel of nontronite also contains more aromatic and/or olefinic carbons (285.0 eV) and much more aliphatic carbons (287.9-288.5 eV) and amide groups (288.2), but less heterocycles (285.9 eV) and less amine/imine/cyano groups and/or ketone and phenol groups (286.5 eV).



336

337 **Figure 5:** XANES spectra of the solid experimental residues.

### 3.5. SEM and TEM

SEM and TEM allowed comparing the textures and microstructures of the solid residues (Figure 6). At the micrometer scale, the solid residue produced in the presence of the crystalline nontronite displays the typical layered, flower-like texture of smectites while the solid residue produced in the presence of the gel of nontronite presents a rough and granular surface. These differences in texture correspond to differences in structure/crystallinity as revealed by TEM observations. At the TEM scale, while stacks of ~5 to ~10 layers (~ 10 nm thick along the 100 direction) extending laterally up to 100 nm can be observed within the solid residue produced in the presence of the crystalline nontronite, much smaller particles (< 10 nm) exhibiting less than 3-5 layers are observed within the solid residue produced in the presence of the gel of nontronite, in good agreement with XRD patterns and MIR data. Besides a few grains of  $\text{Ca}(\text{OH})_2$ , both residues appear homogenous.

No individual organic carbon grain can be observed within the solid residues, but in addition to Fe, Si, O and Ca, STEM-EDS data show that carbon and nitrogen are intimately associated with minerals and homogeneously distributed within the solid residues. Although the starting crystalline nontronite contains Na compensating its permanent charge ( $\text{Na}/\text{Si} = 0.11$ ), the solid residues do not contain any Na, the permanent charge of the smectites being likely compensated by nitrogen (originating from  $\text{NH}_4\text{OH}$ ) and calcium (originating from  $\text{Ca}(\text{OH})_2$ ). The Fe/Si of the solid residues (0.58 and 0.62) are lower than that of the starting crystalline nontronite (0.66). Of note, considering the theoretical formula of nontronite ( $\text{M}^+_{\text{x}}(\text{Fe}_2)(\text{Si}_{4-\text{x}}\text{Fe}_{\text{x}})\text{O}_{10}(\text{OH})_2$ ), the mean  $^{54}\text{Fe}/\text{Si}$  values correspond to permanent charges of 0.2 and 0.28 in the residue produced in the presence of the gel of nontronite and the crystalline nontronite, respectively. The charge of the starting crystalline nontronite was initially 0.4, confirming the interpretation of XRD and MIR results. Based on the study of (Dzene et al., 2017), even for synthetic samples with well-controlled chemistry, permanent

361 tetrahedral charge can be modeled by a distribution heterogeneity as highlighted in figure 6.f. The  
362 distribution of the permanent charge values appears a lot broader for the solid residue produced  
363 from crystalline nontronite compared to the thinner distribution for the solid residue produced from  
364 the nontronite gel.

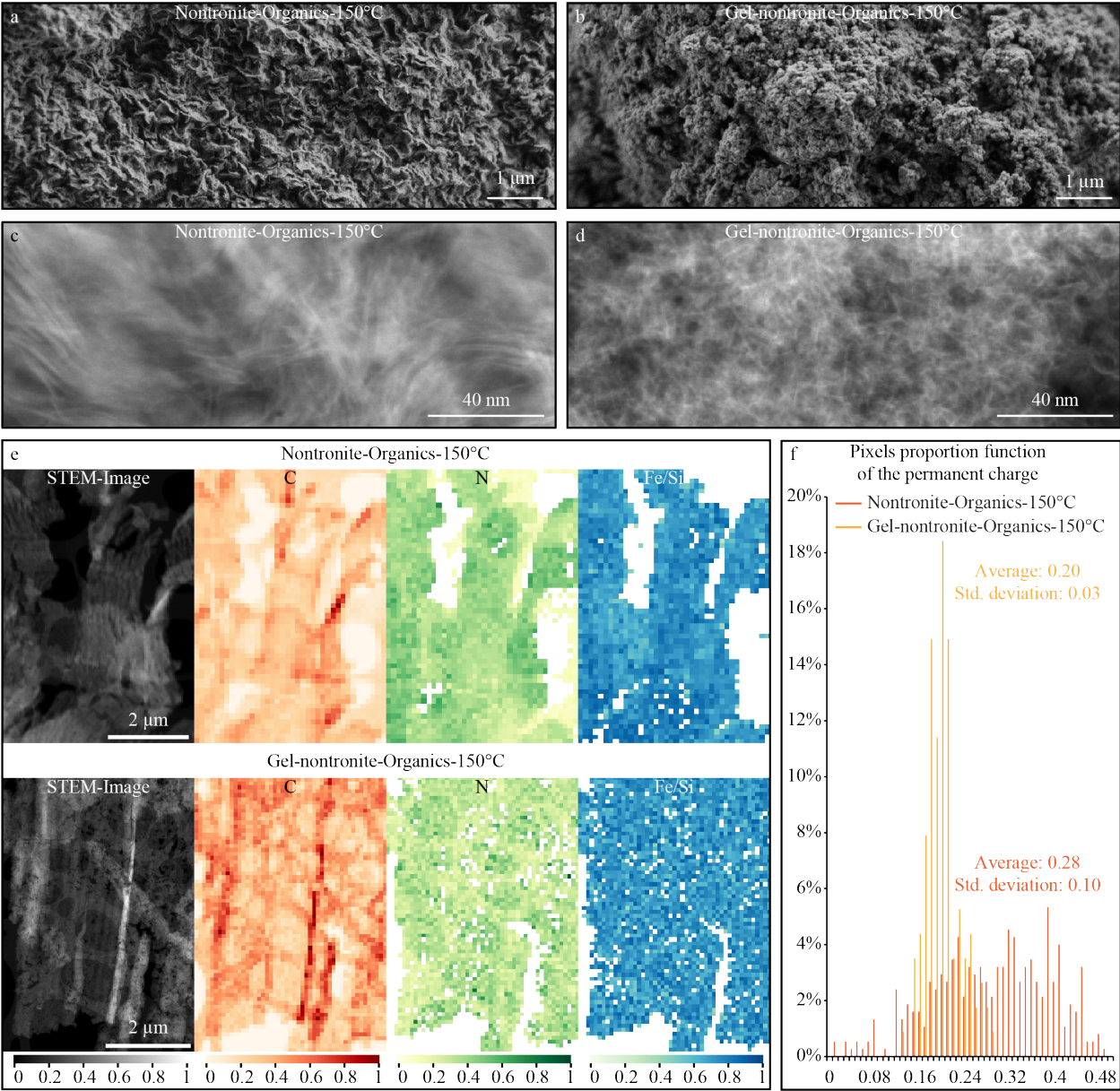


**Figure 6:** (a-b) SEM and (c-d) STEM images of the organo-mineral residues. (e) Chemical maps of organo-mineral residues showing the association of carbon, nitrogen with the Fe-rich smectites and the more heterogeneous Fe/Si ratios of the Nontronite-organics-150°C residue compare to the the Gel-nontronite-organics-150°C residue. (f) Permanent charge distribution of the nontronite highlighting the more homogenous chemical composition of the Gel-nontronite-organics-150°C residue compare to the Nontronite-organics-150°C experiment.

## 4. Discussion

### 4.1. Effect of organo-mineral interactions

In the absence of minerals, the organic mixture produces IOM when exposed to hydrothermal conditions at 150 °C for 3 days. This IOM accounts for ~ 10 % of the initial mass of the organic mixture (see Table 1). According to MIR and XANES data (Figures 4 & 5), this IOM contains aromatic cycles, heterocycles, amine/imine/cyano groups and/or ketone and phenol groups, aliphatic carbons, amide groups and carboxylic groups. The chemical structure of this IOM is thus similar to the organic solids produced in previous studies from the same starting material (Cody et al., 2011; Kebukawa et al., 2013; Kebukawa and Cody, 2015). Similarly to what occurred for HMT (Vinogradoff et al., 2018), the production of IOM from the organic mixture used here occurred via multiple reaction steps, including condensation, dehydration and cyclization reactions involving sugars produced from formaldehyde via the Formose reaction (Kort, 1970; Weber, 2001; Cody et al., 2011; Kebukawa et al., 2013; Kebukawa and Cody, 2015).

However, the present results show that the same mixture does not produce IOM when exposed to similar conditions in the presence of an amorphous gel of nontronite or in the presence of a crystalline nontronite. In fact, no organic solid is retrieved after the acid dissolution of the solid



391 residues investigated here. This is in agreement with results of a previous study, which indicated  
392 that the soluble compounds produced from HMT exposed to hydrothermal conditions in the  
393 presence of smectites have a lower molecular weight than those produced from HMT in the absence  
394 of minerals (Vinogradoff et al., 2020). The DCM-washed solid residues investigated here contain  
395 an important amount of C and N (Table 1), likely under the form of soluble compounds trapped  
396 within the interlayer spaces of smectites (Figure 3) and/or adsorbed at the surface of smectites  
397 (Figure 4). The organic compounds trapped within the residues are not drastically different from  
398 the IOM produced in the absence of minerals from a chemical point of view. Nevertheless, the  
399 organics trapped within the residues produced in the presence of the gel of nontronite are more  
400 aliphatic and contain less phenol carbons (Figure 4 & 5).

401 The presence of organic compounds within the interlayer spaces of the smectites is attested by the  
402 behavior of their 001 d-spacing under vacuum (Figure 3), while the presence of organic compounds  
403 on the edges is attested by the lower absorption of the OH stretching vibrations of water molecules  
404 weakly bonded to the oxygen of the silicate lattice (Figure 4). The quantity of organic compounds  
405 trapped within the solid residues (about 50% of the initial C and more than 60% of the initial N) is  
406 significant considering that only 10 % of the organic mixture is converted into IOM in the absence  
407 of minerals (note that this is not a kinetic limitation - Kebukawa et al., 2013; Kebukawa and Cody,  
408 2015). Such entrapment of nitrogen may have prevented formation of IOM as Kebukawa et al.  
409 (2013) having noticed that high levels of nitrogen yield more IOM. In fact, because OM present in  
410 the liquid phase and the organic compounds trapped within/onto clays minerals share similar  
411 moieties (as revealed by MIR (Figures 1 and 4) and XANES data (Figure 5)), a threshold effect  
412 could be proposed: if the concentration of the reactive species necessary to produce IOM through  
413 polymerization/condensations reactions (Kebukawa et al., 2013) is not high enough, the reaction  
414 may not proceed. Altogether, the present results demonstrate that the presence of smectitic

415 materials, independently of their degree of crystallinity, inhibits the production of IOM. This likely  
416 occurs by trapping organic compounds, hence limiting polymerization/condensation reactions. The  
417 presence of clay minerals has thus a strong influence on reactions between organic species.  
418 The reciprocal is also true. When exposed to hydrothermal conditions at 150 °C for 3 days in the  
419 absence of the organic mixture, the crystalline nontronite remains crystalline while the gel of  
420 nontronite crystallizes (Figures 3 & 4). However, the presence of the organic mixture modifies  
421 these behaviors: the crystallinity of crystalline nontronite decreases during the experiments, while  
422 the gel of nontronite does not produce crystalline nontronite but rather small particles of low degree  
423 of crystallinity (Figures 3, 4 & 6). Similar behaviors were observed in experiments conducted with  
424 gels of (Al,Mg)-rich smectites in the presence of RNA (Jacquemot et al., 2019; Viennet et al., 2019,  
425 2020). As is the case in these studies, the poorly crystalline smectites of the residues investigated  
426 here have retained organic compounds, both within their interlayer spaces (Figure 3 - Viennet et  
427 al., 2019, 2020) and at their surface (Figure 4 - Viennet et al., 2019, 2020). The smectites of the  
428 experimental residues exhibit lower Fe/Si values according to TEM data (Figure 6), indicating that  
429 their permanent charges (corresponding to the number of Si substitutions by <sup>[4]</sup>Fe in the tetrahedral  
430 sheets) is lower than those of the starting crystalline nontronite. Such low permanent charge is also  
431 attested by the MIR results showing a shift of the band position of the Si-O bonds and the relative  
432 intensity decrease of the bands corresponding to the <sup>[4]</sup>Fe-O bonds (Figure 4). The distinct  
433 distribution of the permanent charge values is also of interest. In contrast to the restricted  
434 distribution of the permanent charge values of the solid residue produced in the presence of the gel  
435 of nontronite, the solid residue produced in the presence of the crystalline nontronite exhibits a  
436 rather wide distribution of <sup>[4]</sup>Fe/Si values, i.e. a highly variable permanent charge. By analogy with  
437 the production of lower charge clay minerals via the alteration of micas by organic acids (Jackson,  
438 1962; Robert et al., 1979; Wilson, 1999), it can be assumed that this wide distribution reflects the

alteration by acid-complexation of Fe of the crystalline nontronite during the experiments. While, the sharper distribution of the solid residue produced in the presence of the gel of nontronite would reflect crystallization process from the gel as for smectites produced in inorganic media (Dzene et al., 2017). Of note, in contrast to crystallinity, the permanent charge of nontronites is pH dependent (Baron et al., 2016). The nontronite was synthesized at pH comprise between 12-11.5 (Baron et al., 2016). The presence of  $\text{CaOH}_2$  in the starting materials of our experiments serves as a buffer for a pH at 11.5–11.7 (Kebukawa and Cody, 2015). Yet, such slight decrease of pH would not changes the permanent charge of the nontronites (Baron et al., 2016; Petit et al., 2017). This decrease is likely related to the presence of organic matter. In any case, the present results demonstrate that the presence of organic materials disturbs the crystallization of Fe-rich smectites possibly as observed with (Al,Mg)-rich smectites in the presence of RNA (Jacquemot et al., 2019) and/or via complexation as with iron oxides in soils (Schwertmann, 1966) and affects their permanent charge via the production of organic acids preventing/impacting tetrahedral substitutions (Baron et al., 2016).

#### **4.2. Implications for carbonaceous chondrites**

Asteroid parent bodies accreted organic molecules whose nature and diversity are not yet elucidated, notably because these bodies experienced a multitude of hydrothermal processes, having modified the initial nature of the accreted OM (Cody et al., 2011; Vollmer et al., 2014; Le Guillou and Brearley, 2014; Le Guillou et al., 2014; Vinogradoff et al., 2017). The possible genetic relationships between the SOM and the IOM thus remain a subject of speculations: it has been suggested for instance that soluble compounds have formed via the oxidation of solid (insoluble) organic compounds (Yabuta et al., 2007), that IOM have formed through the polymerization of soluble compounds (Kebukawa et al., 2013; Kebukawa and Cody, 2015; Kebukawa et al., 2020), and that phyllosilicates have played a key role in the chemical evolution of both soluble and

463 insoluble compounds (Le Guillou and Brearley, 2014; Le Guillou et al., 2014; Yesiltas and  
464 Kebukawa, 2016; Changela et al., 2018; Vinogradoff et al., 2020a).

465 The present experimental results provide new clues for understanding the organo-mineral  
466 interactions at work under hydrothermal conditions. In agreement with previous studies (Kebukawa  
467 et al., 2013, 2017, 2020; Kebukawa and Cody, 2015), the production of IOM occurred during  
468 experiments conducted with the organic mixture in the absence of minerals. Yet we show here that  
469 the presence of clay minerals, either amorphous or crystalline, inhibits this production of IOM and  
470 that the organic compounds trapped within the residues are more aliphatic than the IOM. This is  
471 also the case of the diffuse OM intimately associated with clay minerals in chondrites, which has  
472 been documented as more aliphatic than the IOM (Le Guillou and Brearley, 2014; Le Guillou et  
473 al., 2014; Vinogradoff et al., 2017; Changela et al., 2018; Kebukawa et al., 2019; Dionnet et al.,  
474 2020). The present results thus suggest that the chondritic IOM may have only form within pockets  
475 from which clay minerals or amorphous precursors of clay minerals were absent and/or that IOM  
476 grains may have pre-accretionary origins (Remusat et al., 2010).

477 The quantity of organic compounds trapped within the residues investigated here is significantly  
478 higher than that of residues of experiments conducted by Vinogradoff et al. (2020) which produced  
479 residues containing only 3-4 wt % of C. Although these experiments were conducted under similar  
480 conditions, Vinogradoff et al. (2020) used HMT and Al or Fe-rich smectites. Altogether, those  
481 results demonstrate the mutual effect of the crystallochemistry of smectites and the composition of  
482 OM on the composition of the final organo-mineral assemblages. Plus, the present study evidences  
483 that the initial crystallinity of the mineral phase also plays a role in the final chemistry and  
484 quantities of the organic compounds eventually trapped within. The different trapping capacities  
485 of different smectites may explain the highly heterogeneous nature of the matrices of carbonaceous  
486 chondrites, both regarding the crystallochemistry of hydrated silicates and the quantity and

487 chemistry of diffuse OM trapped within these mineral phases (Le Guillou et al., 2014; Vinogradoff  
488 et al., 2017; Changela et al., 2018).

489 The presence of organics partially inhibits the growth of Fe-rich clay minerals such as nontronite  
490 (both the particle sizes and the degree of crystallinity of the smectitic clays are lower in residues  
491 produced in the presence of the organic mixture). Of note, the least altered carbonaceous chondrites  
492 are almost devoid of phyllosilicates and rather contain abundant amorphous silicates (Brearley,  
493 1993; Greshake, 1997; Chizmadia and Brearley, 2008; Abreu and Brearley, 2011; Le Guillou and  
494 Brearley, 2014; Le Guillou et al., 2014, 2015; Dobrică et al., 2019; Dobrică and Brearley, 2020;  
495 Vollmer et al., 2020). Still, these amorphous silicates are intimately associated with diffuse OM,  
496 which is generally interpreted as having been transported by fluids during hydrothermal alteration  
497 episodes (Le Guillou et al., 2014; Vinogradoff et al., 2017; Changela et al., 2018). By analogy with  
498 the present results, it may be suggested that the crystallization of amorphous silicates during  
499 hydrothermal alteration was limited by the presence of organic compounds, while amorphous  
500 silicates occurring in organic-poor regions would have crystallized faster/easier, producing  
501 relatively big particles relatively poor in OM. In addition, the present study suggests that  
502 determining the permanent charge of crystalline phyllosilicates associated to elevated contents of  
503 diffuse OM may bring additional constraints on their origin and history. In fact, according to the  
504 present results, the alteration of pre-existing crystalline phyllosilicates in the presence of organic  
505 compounds should produce smectites exhibiting a highly variable permanent charge while the  
506 crystallization of initially amorphous materials should produce phyllosilicates exhibiting a less  
507 variable permanent charge.

508 Last, it has been suggested that the SOM fraction recovered by solvent extraction does not represent  
509 the entire SOM pool of carbonaceous chondrites (Pearson et al., 2006; Alexander et al., 2017;

510 Vinogradoff et al., 2020a). Here, 50 wt. % of the initial amount of carbon has not been extracted  
511 from the residues using classical solvent extraction. Hence, a significant portion of the chondritic  
512 SOM could have been retained in chondritic clays and disregarded, especially since the abundance  
513 of smectites in carbonaceous chondrites increases with increasing alteration. The present study thus  
514 reinforces the need for *in situ* investigations of OM and/or for the development of new extraction  
515 protocols to better document these -so far- unknown chondritic soluble organic compounds.

## 516 Acknowledgements

517 This work was made possible thanks to financial support from the Agence Nationale de la  
518 Recherche (RAHIIA\_SSOM, ANR-16-CE29-0015) ANR (project RAHIIA\_SSOM – Local PI:  
519 LR) and by the European Research Council for funding via the ERC project HYDROMA  
520 (consolidator grant agreement No. 819587, HYDROMA). This work was supported by the Paris  
521 Île-de-France Region.. We thank Elisabeth Malassis for administrative support, Denis Fiorillo for  
522 his expert support with EA-IRMS, Imène Esteve for her expert support with the SEM. The authors  
523 wish to acknowledge the workforce of the spectroscopic and X-ray diffraction facilities at IMPMC.  
524 Special thanks go to Stefan Stanescu and Sufal Swaraj for their expert support with the HERMES  
525 STXM beamline at SOLEIL. The SEM facility at IMPMC is supported by Region Ile de France  
526 grant SESAME Number I-07-593/R, INSU-CNRS, INP-CNRS and UPMC-Paris 6, and by the  
527 Agence Nationale de la Recherche (ANR) grant number ANR-07-BLAN-0124-01. The TEM  
528 facility at the CCM (Lille University) is supported by the Chevreul Institute, the European FEDER  
529 and Région Nord-Pas-de-Calais. The HERMES beamline (SOLEIL) is supported by the CNRS,  
530 the CEA, the Region Ile de France, the Departmental Council of Essonne and the Region Centre.  
531 Finally, this manuscript has benefited from constructive comments by Dionysis Foustoukos and  
532 one anonymous reviewer , as well as from associate editor Eric Quirico

## 533 References

- 534 Abreu N. M. and Brearley A. J. (2011) Deciphering the nebular and asteroidal record of silicates and organic  
535 material in the matrix of the reduced CV3 chondrite Vigarano: Matrix in the CV3 chondrite  
536 Vigarano. *Meteorit. Planet. Sci.* **46**, 252–274.
- 537 Aléon J. (2010) Multiple origins of nitrogen isotopic anomalies in meteorites and comets. *Astrophys. J.* **722**,  
538 1342–1351.
- 539 Alexander C. M. O., Cody G. D., De Gregorio B. T., Nittler L. R. and Stroud R. M. (2017) The nature,  
540 origin and modification of insoluble organic matter in chondrites, the major source of Earth's C and  
541 N. *Geochemistry* **77**, 227–256.
- 542 Alexander C. M. O., Fogel M., Yabuta H. and Cody G. D. (2007) The origin and evolution of chondrites  
543 recorded in the elemental and isotopic compositions of their macromolecular organic matter.  
544 *Geochim. Cosmochim. Acta* **71**, 4380–4403.
- 545 Aléon J., Bernard S., Le Guillou C., Daval D., Skouri-Panet F., Kuga M. and Robert F. (2017) Organic  
546 molecular heterogeneities can withstand diagenesis. *Sci. Rep.* **7**.
- 547 Baron F., Petit S. and Decarreau A. (2019) Experimental evidence of the metastability of ferric smectite.  
548 *Geochim. Cosmochim. Acta* **265**, 69–84.
- 549 Baron F., Petit S., Tertre E. and Decarreau A. (2016) Influence of Aqueous Si and Fe Speciation on  
550 Tetrahedral Fe(III) Substitutions in Nontronites: a Clay Synthesis Approach. *Clays Clay Miner.* **64**,  
551 230–244.
- 552 Belkhou R., Stanescu S., Swaraj S., Besson A., Ledoux M., Hajlaoui M. and Dalle D. (2015) HERMES: a  
553 soft X-ray beamline dedicated to X-ray microscopy. *J. Synchrotron Radiat.* **22**, 968–979.
- 554 Bernard S., Benzerara K., Beyssac O., Balan E. and Brown Jr. G. E. (2015) Evolution of the macromolecular  
555 structure of sporopollenin during thermal degradation. *Heliyon* **1**, e00034.
- 556 Bernstein M. P., Sandford S. A., Allamandola L. J., Chang S. and Scharberg M. A. (1995) Organic  
557 Compounds Produced by Photolysis of Realistic Interstellar and Cometary Ice Analogs Containing  
558 Methanol. *Astrophys. J.* **454**, 327.
- 559 Blazzevjic N., Kolbah D., Belin B., Sunjic V. and Kajfez F. (1979) Hexamethylenetetramine, A Versatile  
560 Reagent in Organic Synthesis. *Synthesis* **1979**, 161–176.
- 561 Brearley A. J. (2006) The action of water. In *Meteorites and the Early Solar System II* (eds. D. S. Lauretta  
562 and H. Y. McSween). University of Arizona Press, Tucson, pp. 587–624.
- 563 Brearley A. J. (1993) Matrix and fine-grained rims in the unequilibrated CO3 chondrite, ALHA77307:  
564 Origins and evidence for diverse, primitive nebular dust components. *Geochim. Cosmochim. Acta*  
565 **57**, 1521–1550.
- 566 Changela H. G., Le Guillou C., Bernard S. and Brearley A. J. (2018) Hydrothermal evolution of the  
567 morphology, molecular composition, and distribution of organic matter in CR (Renazzo-type)  
568 chondrites. *Meteorit. Planet. Sci.* **53**, 1006–1029.
- 569 Chizmadia L. J. and Brearley A. J. (2008) Mineralogy, aqueous alteration, and primitive textural  
570 characteristics of fine-grained rims in the Y-791198 CM2 carbonaceous chondrite: TEM  
571 observations and comparison to ALHA81002. *Geochim. Cosmochim. Acta* **72**, 602–625.
- 572 Cliff G. and Lorimer G. W. (1975) The quantitative analysis of thin specimens. *J. Microsc.* **103**, 203–207.
- 573 Cody G. D. and Alexander C. M. O. 'D. (2005) NMR studies of chemical structural variation of insoluble  
574 organic matter from different carbonaceous chondrite groups. *Geochim. Cosmochim. Acta* **69**,  
575 1085–1097.
- 576 Cody G. D., Heying E., Alexander C. M. O., Nittler L. R., Kilcoyne A. L. D., Sandford S. A. and Stroud R.  
577 M. (2011) Establishing a molecular relationship between chondritic and cometary organic solids.  
578 *Proc. Natl. Acad. Sci. U. S. A.* **108**, 19171–19176.
- 579 Cottin H., Szopa C. and Moore M. H. (2001) Production of Hexamethylenetetramine in Photolyzed and  
580 Irradiated Interstellar Cometary Ice Analogs. *Astrophys. J.* **561**, L139–L142.



- Danger G., Vinogradoff V., Matzka M., Viennet J.-C., Remusat L., Bernard S., Ruf A., Le Sergeant d'Hendecourt L. and Schmitt-Kopplin P. (2021) Exploring the link between molecular cloud ices and chondritic organic matter in laboratory. *Nat. Commun.* **12**, 3538.
- Derenne S. and Robert F. (2010) Model of molecular structure of the insoluble organic matter isolated from Murchison meteorite: Model of molecular structure of Murchison IOM. *Meteorit. Planet. Sci.* **45**, 1461–1475.
- Dionnet Z., Aleon-Toppani A., Baklouti D., Borondics F., Brisset F., Djouadi Z., Sandt C. and Brunetto R. (2018) Organic and mineralogic heterogeneity of the Paris meteorite followed by FTIR hyperspectral imaging. *Meteorit. Planet. Sci.* **53**, 2608–2623.
- Dionnet Z., Brunetto R., Aléon-Toppani A., Rubino S., Baklouti D., Borondics F., Buellet A.-C., Djouadi Z., King A., Nakamura T., Rotundi A., Sandt C., Troadec D. and Tsuchiyama A. (2020) Combining IR and X-ray microtomography data sets: Application to Itokawa particles and to Paris meteorite. *Meteorit. Planet. Sci.* **55**, 1645–1664.
- Dobrică E. and Brearley A. J. (2020) Amorphous silicates in the matrix of Semarkona: The first evidence for the localized preservation of pristine matrix materials in the most unequilibrated ordinary chondrites. *Meteorit. Planet. Sci.* **55**, 649–668.
- Dobrică E., Le Guillou C. and Brearley A. J. (2019) Aqueous alteration of porous microchondrules in Semarkona: Implications for hydration, oxidation and elemental exchange processes. *Geochim. Cosmochim. Acta* **244**, 292–307.
- Dzene L., Verron H., Delville A., Michot L. J., Robert J.-L., Tertre E., Hubert F. and Ferrage E. (2017) Influence of Tetrahedral Layer Charge on the Fixation of Cesium in Synthetic Smectite. *J. Phys. Chem. C* **121**, 23422–23435.
- Farmer V. C. ed. (1974) The Infrared Spectra of Minerals. *Mineralogical Society of Great Britain and Ireland*.
- Farmer V. C. and Russell J. D. (1971) Interlayer complexes in layer silicates. The structure of water in lamellar ionic solutions. *Trans. Faraday Soc.* **67**, 2737.
- Foustoukos D. I. and Stern J. C. (2012) Oxidation pathways for formic acid under low temperature hydrothermal conditions: Implications for the chemical and isotopic evolution of organics on Mars. *Geochim. Cosmochim. Acta* **76**, 14–28.
- Garvie L. A. J. and Buseck P. R. (2007) Prebiotic carbon in clays from Orgueil and Ivuna (CI), and Tagish Lake (C2 ungrouped) meteorites. *Meteorit. Planet. Sci.* **42**, 2111–2117.
- Gautier M., Muller F. and Le Forestier L. (2017) Interactions of ammonium-smectite with volatile organic compounds from leachates. *Clay Miner.* **52**, 143–158.
- Greshake A. (1997) The primitive matrix components of the unique carbonaceous chondrite Acfer 094: A TEM study. *Geochim. Cosmochim. Acta* **61**, 437–452.
- Jackson M. L. (1962) Interlayering of Expansible Layer Silicates in Soils by Chemical Weathering. *Clays Clay Miner.* **11**, 29–46.
- Jacquemot P., Viennet J.-C., Bernard S., Le Guillou C., Rigaud B., Delbes L., Georgelin T. and Jaber M. (2019) The degradation of organic compounds impacts the crystallization of clay minerals and vice versa. *Sci. Rep.* **9**, 20251.
- Kebukawa Y., Chan Q. H. S., Tachibana S., Kobayashi K. and Zolensky M. E. (2017) One-pot synthesis of amino acid precursors with insoluble organic matter in planetesimals with aqueous activity. *Sci. Adv.* **3**, e1602093.
- Kebukawa Y. and Cody G. D. (2015) A kinetic study of the formation of organic solids from formaldehyde: Implications for the origin of extraterrestrial organic solids in primitive Solar System objects. *Icarus* **248**, 412–423.
- Kebukawa Y., David Kilcoyne A. L. and Cody G. D. (2013) Exploring the Potential Formation of Organic Solids in Chondrites and Comets through Polymerization of Interstellar Formaldehyde. *Astrophys. J.* **771**, 19.

630 Kebukawa Y., Kobayashi H., Urayama N., Baden N., Kondo M., Zolensky M. E. and Kobayashi K. (2019)  
631 Nanoscale infrared imaging analysis of carbonaceous chondrites to understand organic-mineral  
632 interactions during aqueous alteration. *Proc. Natl. Acad. Sci. U. S. A.* **116**, 753–758.

633 Kebukawa Y., Nakashima S., Mita H., Muramatsu Y. and Kobayashi K. (2020) Molecular evolution during  
634 hydrothermal reactions from formaldehyde and ammonia simulating aqueous alteration in meteorite  
635 parent bodies. *Icarus* **347**, 113827.

636 Kerridge J. F. (1993) Origins of organic matter in meteorites. *Proceedings of the NIPR Symposium on*  
637 *Antarctic meteorites* **6**, pp. 293–303.

638 King A. J., Schofield P. F., Howard K. T. and Russell S. S. (2015) Modal mineralogy of CI and CI-like  
639 chondrites by X-ray diffraction. *Geochim. Cosmochim. Acta* **165**, 148–160.

640 Kort M. J. (1970) Reactions of Free Sugars with Aqueous Ammonia. In *Advances in Carbohydrate*  
641 *Chemistry and Biochemistry* Elsevier. pp. 311–349.

642 Lagaly G., Ogawa M. and Dékány I. (2013) Chapter 10.3 - Clay Mineral–Organic Interactions. In  
643 *Developments in Clay Science* (eds. F. Bergaya and Gerhard Lagaly). Handbook of Clay Science.  
644 Elsevier. pp. 435–505.

645 Laird D. A. (1994) Evaluation of the Structural Formula and Alkylammonium Methods of Determining  
646 Layer Charge. In *Layer Charge Characteristics of 2:1 Silicate Clay Minerals*, Clay Minerals  
647 Society.

648 Le Guillou C., Bernard S., Brearley A. J. and Remusat L. (2014) Evolution of organic matter in Orgueil,  
649 Murchison and Renazzo during parent body aqueous alteration: In situ investigations. *Geochim.*  
650 *Cosmochim. Acta* **131**, 368–392.

651 Le Guillou C., Bernard S., De la Pena F. and Le Brech Y. (2018) XANES-Based Quantification of Carbon  
652 Functional Group Concentrations. *Anal. Chem.* **90**, 8379–8386.

653 Le Guillou C. and Brearley A. (2014) Relationships between organics, water and early stages of aqueous  
654 alteration in the pristine CR3.0 chondrite MET 00426. *Geochim. Cosmochim. Acta* **131**, 344–367.

655 Le Guillou C., Changela H. G. and Brearley A. J. (2015) Widespread oxidized and hydrated amorphous  
656 silicates in CR chondrites matrices: Implications for alteration conditions and H<sub>2</sub> degassing of  
657 asteroids. *Earth Planet. Sci. Lett.* **420**, 162–173.

658 Lewan M. D. (1997) Experiments on the role of water in petroleum formation. *Geochim. Cosmochim. Acta*  
659 **61**, 3691–3723.

660 Lewan M. D. and Roy S. (2011) Role of water in hydrocarbon generation from Type-I kerogen in Mahogany  
661 oil shale of the Green River Formation. *Org. Geochem.* **42**, 31–41.

662 McCollom T. M. (2013) The influence of minerals on decomposition of the n-alkyl- $\alpha$ -amino acid norvaline  
663 under hydrothermal conditions. *Geochim. Cosmochim. Acta* **104**, 330–357.

664 McCollom T. M., Lollar B. S., Lacrampe-Couloume G. and Seewald J. S. (2010) The influence of carbon  
665 source on abiotic organic synthesis and carbon isotope fractionation under hydrothermal conditions.  
666 *Geochim. Cosmochim. Acta* **74**, 2717–2740.

667 Mccollom T. and Seewald J. (2006) Carbon isotope composition of organic compounds produced by abiotic  
668 synthesis under hydrothermal conditions. *Earth Planet. Sci. Lett.* **243**, 74–84.

669 McSween H. Y. (1979) Alteration in CM carbonaceous chondrites inferred from modal and chemical  
670 variations in matrix. *Geochim. Cosmochim. Acta* **43**, 1761–1770.

671 Meissner F., Schwiedessen E. and Othmer D. F. (1954) Continuous Production of Hexamethylenetetramine.  
672 *Ind. Eng. Chem.* **46**, 724–727.

673 Morris P. L. (1980) The correction of thin foil microanalysis data for X-ray absorption effects. *Electron*  
674 *Microscopy and Analysis 1979*, 413–416.

675 Nagendrappa G. (2011) Organic synthesis using clay and clay-supported catalysts. *Appl. Clay Sci.* **53**, 106–  
676 138.

677 Nagendrappa G. and Chowreddy R. R. (2021) Organic Reactions Using Clay and Clay-Supported Catalysts:  
678 A Survey of Recent Literature. *Catal. Surv. Asia* **25**, 231–278.

- Nittler L. R., Stroud R. M., Trigo-Rodríguez J. M., De Gregorio B. T., Alexander C. M. O., Davidson J., Moyano-Cambero C. E. and Tanbakouei S. (2019) A cometary building block in a primitive asteroidal meteorite. *Nat. Astron.* **3**, 659–666.
- Pan C., Geng A., Zhong N., Liu J. and Yu L. (2009) Kerogen pyrolysis in the presence and absence of water and minerals: Amounts and compositions of bitumen and liquid hydrocarbons. *Fuel* **88**, 909–919.
- Pearson V. K., Sephton M. A., Franchi I. A., Gibson J. M. and Gilmour I. (2006) Carbon and nitrogen in carbonaceous chondrites: Elemental abundances and stable isotopic compositions. *Meteorit. Planet. Sci.* **41**, 1899–1918.
- de la Pena F., Ostasevicius T., Tonaas Fauske V., Burdet P., Jokubauskas P., Nord M., Sarahan M., Prestat E., Johnstone D. N., Taillon J., Jan Caron, Furnival T., MacArthur K. E., Eljarrat A., Mazzucco S., Migunov V., Aarholt T., Walls M., Winkler F., Donval G., Martineau B., Garmannslund A., Zagonel L.-F. and Iyengar I. (2017) Electron Microscopy (Big and Small) Data Analysis With the Open Source Software Package HyperSpy. *Microsc. Microanal.* **23**, 214–215.
- Petit S., Baron F. and Decarreau A. (2017) Synthesis of nontronite and other Fe-rich smectites: a critical review. *Clay Miner.* **52**, 469–483.
- Pizzarello S., Cooper G. W. and Flynn G. J. (2006) The nature and distribution of the organic material in carbonaceous chondrites and interplanetary dust particles. *Meteorites and the early solar system II* **1**, 625–651.
- Remusat L. (2015) Organics in primitive meteorites. *EMU notes in Mineralogy* **15**, 33–65.
- Remusat L., Bonnet J.-Y., Bernard S., Buch A. and Quirico E. (2019) Molecular and isotopic behavior of insoluble organic matter of the Orgueil meteorite upon heating. *Geochim. Cosmochim. Acta* **263**, 235–247.
- Remusat L., Derenne S. and Robert F. (2005a) New insight on aliphatic linkages in the macromolecular organic fraction of Orgueil and Murchison meteorites through ruthenium tetroxide oxidation. *Geochim. Cosmochim. Acta* **69**, 4377–4386.
- Remusat L., Derenne S., Robert F. and Knicker H. (2005b) New pyrolytic and spectroscopic data on Orgueil and Murchison insoluble organic matter: A different origin than soluble? *Geochim. Cosmochim. Acta* **69**, 3919–3932.
- Remusat L., Guan Y., Wang Y. and Eiler J. M. (2010) Accretion and preservation of D-rich organic particles in carbonaceous chondrites: evidence for important transport in the early Solar System nebula. *Astrophys. J.* **713**, 1048–1058.
- Remusat L., Robert F., Meibom A., Mostefaoui S., Delpoux O., Binet L., Gourier D. and Derenne S. (2009) Proto-planetary disk chemistry recorded by D-rich organic radicals in carbonaceous chondrites. *Astrophys. J.* **698**, 2087–2092.
- Ricardo A. (2004) Borate Minerals Stabilize Ribose. *Science* **303**, 196–196.
- Robert F. and Epstein S. (1982) The concentration and isotopic composition of hydrogen, carbon and nitrogen in carbonaceous meteorites. *Geochim. Cosmochim. Acta* **46**, 81–95.
- Robert M., Razzaghe M., Vicente M. A. and Veneau G. (1979) Role du facteur biochimique dans l'alteration des minéraux silicates. *Bulletin de l'Association Française pour l'Etude du Sol*, 153–174.
- Schwertmann U. (1966) Inhibitory Effect of Soil Organic Matter on the Crystallization of Amorphous Ferric Hydroxide. *Nature* **212**, 645–646.
- Seewald J. S. (2001) Aqueous geochemistry of low molecular weight hydrocarbons at elevated temperatures and pressures: constraints from mineral buffered laboratory experiments. *Geochim. Cosmochim. Acta* **65**, 1641–1664.
- Sephton M. A. (2014) Organic Geochemistry of Meteorites. In *Treatise on Geochemistry (Second Edition)* (eds. H. D. Holland and K. K. Turekian). Elsevier, Oxford. pp. 1–31.
- Swaraj S., Belkhou R., Stanescu S., Rioult M., Besson A. and Hitchcock A. P. (2017) Performance of the HERMES beamline at the carbon K-edge. *Journal of Physics: Conference Series* **849**, 012046.
- Viennet J.-C., Bernard S., Le Guillou C., Jacquemot P., Balan E., Delbes L., Rigaud B., Georgelin T. and Jaber M. (2019) Experimental clues for detecting biosignatures on Mars. *Geochem. Persp. Lett.*, 28–33.

- Viennet J.-C., Bernard S., Le Guillou C., Jacquemot P., Delbes L., Balan E. and Jaber M. (2020) Influence of the nature of the gas phase on the degradation of RNA during fossilization processes. *Appl. Clay Sci.* **191**, 105616.
- Viennet J.-C., Hubert F., Ferrage E., Tertre E., Legout A. and Turpault M.-P. (2015) Investigation of clay mineralogy in a temperate acidic soil of a forest using X-ray diffraction profile modeling: Beyond the HIS and HIV description. *Geoderma* **241–242**, 75–86.
- Viennet J.-C., Hubert F., Tertre E., Ferrage E., Robin V., Dzene L., Cochet C. and Turpault M.-P. (2016) Effect of particle size on the experimental dissolution and auto-aluminization processes of K-vermiculite. *Geochim. Cosmochim. Acta* **180**, 164–176.
- Vinogradoff V., Bernard S., Le Guillou C. and Remusat L. (2018) Evolution of interstellar organic compounds under asteroidal hydrothermal conditions. *Icarus* **305**, 358–370.
- Vinogradoff V., Duvernay F., Danger G., Theulé P. and Chiavassa T. (2011) New insight into the formation of hexamethylenetetramine (HMT) in interstellar and cometary ice analogs. *Astronomy & Astrophysics* **530**, A128.
- Vinogradoff V., Le Guillou C., Bernard S., Binet L., Cartigny P., Brearley A. J. and Remusat L. (2017) Paris vs. Murchison: Impact of hydrothermal alteration on organic matter in CM chondrites. *Geochim. Cosmochim. Acta* **212**, 234–252.
- Vinogradoff V., Le Guillou C., Bernard S., Viennet J.-C., Jaber M. and Remusat L. (2020a) Influence of phyllosilicates on the hydrothermal alteration of organic matter in asteroids: Experimental perspectives. *Geochim. Cosmochim. Acta* **269**, 150–166.
- Vinogradoff V., Remusat L., McLain H. L., Aponte J. C., Bernard S., Danger G., Dworkin J. P., Elsila J. E. and Jaber M. (2020b) Impact of Phyllosilicates on Amino Acid Formation under Asteroidal Conditions. *ACS Earth Space Chem.* **4**, 1398–1407.
- Vollmer C., Kepaptsoglou D., Leitner J., Busemann H., Spring N. H., Ramasse Q. M., Hoppe P. and Nittler L. R. (2014) Fluid-induced organic synthesis in the solar nebula recorded in extraterrestrial dust from meteorites. *Proc. Natl. Acad. Sci. U. S. A.* **111**, 15338–15343.
- Vollmer C., Leitner J., Kepaptsoglou D., Ramasse Q. M., Busemann H. and Hoppe P. (2020) Isotopic compositions, nitrogen functional chemistry, and low-loss electron spectroscopy of complex organic aggregates at the nanometer scale in the carbonaceous chondrite Renazzo. *Meteorit. Planet. Sci.* **55**, 1293–1319.
- Wang J., Morin C., Li L., Hitchcock A. P., Scholl A. and Doran A. (2009) Radiation damage in soft X-ray microscopy. *J. Electron Spectrosc. Relat. Phenom.* **170**, 25–36.
- Weber A. L. (2001) The Sugar Model: Catalysis by Amines and Amino Acid Products. *Orig. Life Evol. Biosph.* **31**, 71–86.
- Wilson M. J. (1999) The origin and formation of clay minerals in soils: past, present and future perspectives. *Clay miner.* **34**, 7–25.
- Yabuta H., Williams L. B., Cody G. D., Alexander C. M. O. and Pizzarello S. (2007) The insoluble carbonaceous material of CM chondrites: A possible source of discrete organic compounds under hydrothermal conditions. *Meteorit. Planet. Sci.* **42**, 37–48.
- Yariv S. and Cross H. (2001) *Organo-clay complexes and interactions*. CRC Press.
- Yesiltas M. and Kebukawa Y. (2016) Associations of organic matter with minerals in Tagish Lake meteorite via high spatial resolution synchrotron-based FTIR microspectroscopy. *Meteorit. Planet. Sci.* **51**, 584–595.